



Spatiotemporal changes in hurricane-force wind risk assessment in the Yucatan Peninsula, Mexico

David Romero¹ · José Francisco León-Cruz²

Received: 14 June 2023 / Accepted: 26 December 2023 / Published online: 24 January 2024
© The Author(s) 2024

Abstract

Tropical cyclones are one of the most dangerous natural phenomena. These extreme events involve various hazards, such as strong winds, severe precipitation, storm surge, flooding, and landslides. In Mexico, tropical cyclones are the most frequent natural threats and have a high cost to affected populations. This research aimed to characterise the spatial and temporal changes in risk associated with hurricane winds on the Yucatan Peninsula. This effort included a comprehensive analysis of three integral risk components (hazard, vulnerability, and exposure) for three distinct time intervals (1950–2000, 1950–2010, and 1950–2020). This analytical process was executed utilising a fine-resolution hexagonal grid. Hazard was estimated by calculating the probabilities of occurrence of winds related to various hurricane categories after estimating wind fields from the International Best Track Archive for Climate Stewardship (IBTrACS) data with a parametric model. Vulnerability was approximated by constructing indicators with sociodemographic data from the National Population and Housing Census issued by Mexico's National Institute of Statistics and Geography. With these indicators, a factor analysis was performed, and a weighted index was constructed. Finally, exposure was estimated from population density. Each of these indices was aggregated at the hexagonal level, allowing the calculation of the risk associated with hurricane-force wind. The results showed high-risk levels associated with high-hazard levels, e.g. in coastal areas such as the Riviera Maya. Similarly, high-risk levels are related to high marginalisation, i.e. vulnerability, in the northeastern zone of the Yucatan Peninsula. The increased frequency of tropical cyclones combined with high population densities has recently led to higher risk levels in this region of Mexico.

Keywords Tropical cyclones · Hazard · Vulnerability · Exposure · Spatial changes · Hexagon grid

✉ David Romero
dromero@enesmerida.unam.mx

¹ Escuela Nacional de Estudios Superiores Unidad Mérida, Universidad Nacional Autónoma de México, Ucu 97357, México

² Departamento de Geografía Física, Instituto de Geografía, Universidad Nacional Autónoma de México, Ciudad Universitaria, Mexico City 04510, México

1 Introduction

The cost of disasters is growing continuously worldwide (CRED 2022); among these, tropical cyclones (TCs) have the most significant socioeconomic impact on North America and Mesoamerica coastal regions. The adverse effects of TCs depend on several factors, including the location of economic activities, the total production and capital of these activities, the number and intensity of TCs, and the geographic characteristics of the affected areas (Nordhaus 2006). For example, the National Oceanic and Atmospheric Administration (NOAA) issues annual estimates of the economic impacts of tropical cyclones in the US. The estimated total damage was USD 417.9 billion in 2013, approximately USD 530 billion in 2015, and USD 945.9 billion in 2019. The destruction associated with the effects of TCs is evident and increasing. On the other hand, according to the EM-Dat database between 2000 and 2022 (CRED 2022), 52.8% of the total number of records (37) in the Yucatan Peninsula (YP) correspond to TCs, which represented 73% of disasters related to natural hazards, demonstrating the importance of these phenomena in the region.

YP is one of the regions of Mexico with the highest frequency of occurrence of TC (Farfán et al. 2014). The estimated cost of the TCs that hit the region revealed a total economic loss of USD 2 402 million for hurricane (H) “Wilma” in 2005—the latest major event to reach the area—and USD 1 166 million for “Gilbert” in 1988, according to the Mexican Insurance Association (*Asociación Mexicana de Instituciones de Seguros*, AMIS) (2021). For the latter, authorities reported 202 human deaths in the YP (Lawrence and Gross 1989). Globally, economic losses from TCs are much higher than a few decades ago due to the expansion of infrastructure in coastal areas (Homewood 2019). This growing coastal infrastructure (related to exposure) in areas of high incidence of hazardous phenomena (e.g. TCs) is one of the main drivers of the disaster risk associated with these meteorological events.

The risk concept has been studied from numerous approaches and disciplines, having experienced various changes over time (Accastello et al. 2021). Given the nature of the phenomenon analysed herein, we selected the framework provided by the Intergovernmental Panel on Climate Change (IPCC 2012) for this study. In this sense, disaster risk can be summarised as “the likelihood, over a specified time lapse, of severe alterations in the normal functioning of a community or a society due to hazardous physical events interacting with vulnerable social conditions, leading to widespread adverse human, material, economic, or environmental effects”. Three main risk components are identified above: vulnerability (predisposition to suffer damage), exposure (presence of population, livelihoods, and resources that could be affected), and hazard (potential occurrence of a natural or anthropogenic phenomenon that may cause damage) (IPCC 2012; Kamranzad et al. 2020). These concepts involve various assumptions, many of which are extremely difficult to quantify. Risk assessment can be considered a simplified approach that is particularly useful on large scales.

In natural phenomena such as TCs (the hazard component), two fundamental elements allow evaluating their potential threat: frequency and intensity (Shi et al. 2020). The first is defined as the number of times a catastrophe occurs per unit of time; the second represents the strength of a phenomenon in a given place. In Mexico and its surrounding areas, intensity is measured using the Saffir–Simpson scale based on sustained wind speed for 1 min. Tropical storms have 1-min sustained winds of at least 34 knots (17.34 m s^{-1}), while Hs are characterised by sustained winds of at least 64 knots (32.64 m s^{-1}). In the YP and its surrounding areas, the maximum wind speed ever recorded is 165 knots (84.15 m s^{-1})

associated with H "Allen", which passed 40 km offshore of Quintana Roo in the Yucatan Channel in 1980. The peak landfall wind speed to date is 150 knots ($76.50 \text{ m}\cdot\text{s}^{-1}$), recorded when H "Janet" struck southern Quintana Roo in 1955.

The study of vulnerability to natural phenomena such as TCs has been a recurring subject addressed in the specialised literature in Mexico and worldwide (e.g. Pielke et al. 2003; Pita et al. 2013; Marín-Monroy et al. 2020; Boragapu et al. 2023). These investigations have sought to explain the role of the socioenvironmental conditions of human populations in defining the probability of damage. Changes in economic, political, and cultural conditions, among others, are critical to determining the role of society in the generation of risk situations and the probability of disaster occurrence. Some studies in Mexico have addressed the elements of vulnerability to TCs at local, regional, and even national scales (e.g. Guzmán Noh and Rodríguez Esteves 2016; García-Benítez and Adame-Martínez 2017). Similarly, Mexico's National Centre for Disaster Prevention (*Centro Nacional de Prevención de Desastres*; CENAPRED) has established a social vulnerability index to estimate TC-related risk in the country (CENAPRED 2015).

It is worth noting that risk indices require continuous updating, since vulnerability, exposure, and hazard are not static components. A multiannual risk assessment of natural hazards is essential to understand changes in risk components and their implications for potential disasters. Previous research has focused on vulnerability's spatial and temporal changes (e.g. Cutter and Finch 2008; Bronfman et al. 2021) and hazard (e.g. Nie et al. 2012; Dahal et al. 2016). In Mexico, no studies have evaluated spatial and temporal changes in the risk of natural hazards and its components, let alone studies assessing the exposure, vulnerability, and hazard to hurricanes (one of the country's most common and dangerous threats) at the local level.

In this context, the present investigation characterised the risk associated with hurricanes in the YP. We used an approach where risk is the product of hazard, exposure, and vulnerability. After calculating these risk components, we investigated the spatiotemporal changes (years 2000, 2010, and 2020) of hurricane-force wind risk in the YP. Section two details the data sources and methods used to construct the indices. Section 3 describes and discusses the results obtained based on the spatial distribution of the different risk components computed. Finally, conclusions are drawn from our key findings.

2 Study area

The YP is located in eastern Mexico between the Gulf of Mexico and the Caribbean Sea (Fig. 1). This region comprises three states: Yucatan, Quintana Roo, and Campeche. The study area covers approximately $137,600 \text{ km}^2$, excluding water bodies, representing around 7.1% of the Mexican territory. This part of the country borders Guatemala and Belize to the south and east. According to the latest national census, the three states just mentioned are home to about 5 million inhabitants—around 4% of the total population in Mexico (*Instituto Nacional de Estadística y Geografía*; INEGI 2021). This area has undergone significant tourism development in recent years, mainly in the region known as the Riviera Maya (García de Fuentes et al. 2019).

Extensive plains with no significant elevations characterise the YP. Given its geographic location, this region is prone to the impact of tropical cyclones, easterly waves, and cold fronts (Mendoza et al. 2013; Dominguez and Magaña 2018). The precipitation regime is characterised by two well-defined seasons: a summer wet season with bimodal

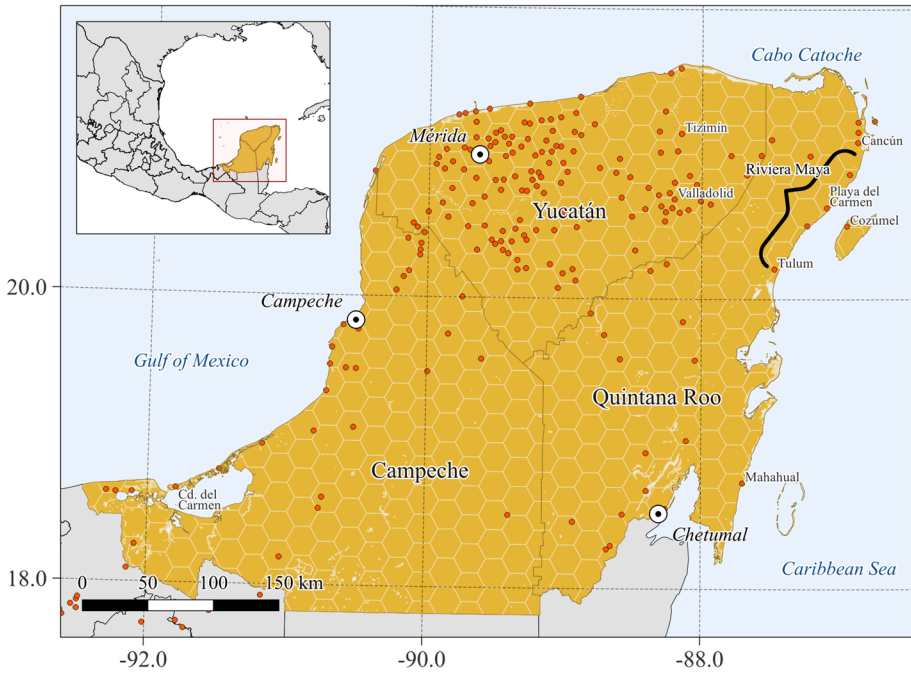


Fig. 1 Map of the study area. White circles indicate state capitals; red dots mark urban areas

precipitations (García-Franco et al. 2023) and a dry season the rest of the year; the relative duration of both seasons is spatially variable in the peninsula (Romero et al. 2020).

Many TCs have historically hit this region (Farfán et al. 2014; Rivera-Monroy et al. 2020), making it a high-risk area for tropical systems. Previous studies have noted that the northern area of the peninsula, between the states of Quintana Roo and Yucatan, is where more storms have impacted from 1851 to 2000 (Boose et al. 2003). Various major Hs, such as "Janet" (in 1955), "Gilbert" (in 1988), and "Wilma" (in 2005), have demonstrated the damaging potential of these natural phenomena in this part of the country. Some studies mention that under a warming scenario, the YP would be increasingly susceptible to more frequent strong Hs and more regular events that undergo rapid intensification (Appendini et al. 2019).

3 Data and methodology

3.1 Hazard index

Tropical cyclone data were obtained from the North Atlantic database of the International Best Track Archive for Climate Stewardship (IBTrACS) Project, version 4 (Knapp et al. 2010, 2018). Shapefiles contain information for the TCs recorded between 1851 and 2022 in the North Atlantic area. The database contains 123 321 records. The relevant data for the study zone include the agency responsible for the data, geographic position (in degrees, with two decimal places), system number, code number, date and time, maximum

sustained wind speed (in knots), and distance to land. Additional data, such as atmospheric pressure, are not available for all records. For the study area, data from the World Meteorological Organisation are available for use, recorded at six-hour intervals and with wind speeds reported in multiples of five. Also available are data from the National Hurricane Centre (NHC) corresponding to a window of three hours maximum. Although most wind data are also reported in multiples of five, the maximum speed zones of each system are usually more accurate. We obtained the points layer relative to the location of the TC eye at the time of recording. The 1950–2020 data period was selected for the present analysis because the reliable time series for tropical cyclones began in the mid-1940s when the H hunter aircraft started operations (Neumann and Elms 1993; Landsea and Franklin 2013).

The hazard related to hurricane-force wind was evaluated based on the probability of occurrence of these conditions in the study area. Several methodologies were used to convert all the IBTrACS points with selected wind speeds into hurricane-force wind fields to consider the relative impact zones of each cyclone.

From the IBTrACS points, we interpolated the TC characteristics and location with splines at a 1-h time scale (Horinouchi et al. 2020). Distances between the trajectory point and the hurricane-force wind field limit were calculated using the parametric model of Holland (1980) corrected for surface wind (Ruiz-Salcines et al. 2019). We computed the wind field at each 1-h eye position and then extracted the profile at 90° (right and left) with respect to the translation direction. From that profile, we obtained the geographic position of the 64-kt wind speed and calculated the distance to the trajectory point, in metres. Due to the high asymmetry of TC wind fields (Nederhoff et al. 2019), the method could give zero distance values for systems with maximum sustained winds up to 80 kt. However, this distance is greater locally (Figs. s1 and s2). To solve this issue, we also computed the distances for sustained wind speeds of 32 kt, calculated the asymmetry quotient for these winds, and applied it to distances of 64 kt to the right to obtain the relative radius to the left, as needed.

One-hour trajectories were built from coordinate points and buffers were created considering the differences between sides that were later joined to create a wind-field polygon for each H.

Subsequently, we calculated the probability of occurrence of hurricane-force wind by counting the presence of wind fields per homogeneous territorial unit throughout the study area. The above was carried out using a hexagonal grid—the most appropriate design for this purpose (Elsner et al. 2012). The cells had a 0.2° opening as we sought a fine resolution to identify those areas facing a higher risk. Additionally, this size, which provides complete cells of approximately 400 km² (331 km² on average), is similar to the median size of municipalities in the study area. It is worth highlighting that all spatial units comprised almost the same area, except for those with either coastal limits or a water body (lake/lagoon) within the cell. To avoid latitudinal biases related to geographic projections in the area and density calculations, the grid was created with the *sf* package in R and the Universal Transverse Mercator projection for zone 16 North with World Geodesic System 1984 datum, the system most commonly used to map the Yucatan Peninsula at a regional scale. The generated grid was used to calculate the hazard, vulnerability, exposure, and risk indices. The grid was joined in the Geographic Information System with layers of wind fields after transforming them by changing the projection system. Afterwards, the resulting layers were dissolved according to cells, counting the number of crossed wind fields in each; also, the number of annual occurrences was divided by three, as we used three different radii to model the wind fields for each H. Finally, the annual probabilities of occurrence (P_H) in the tropical storm and H categories were calculated considering the Poisson

distribution, the most adapted probability model to describe the data count (Elsner and Jagger 2013). The equation used was the following (Eq. 1):

$$P_H = 1 - \exp\left(\frac{-n}{t}\right) \quad (1)$$

where n is the number of wind fields recorded during the time lapse t (in years).

The annual H hazard index (HI_y) was determined based on the quintiles of probability values from the dataset that includes the three periods analysed; probabilities equal to 0 (zero), which represent no hazard, were excluded from the analysis. Thus, hazard levels correspond to integers from zero to five. We also applied wind field modelling for H trajectories between 1851 and 1950. Finally, we assigned a hazard level of 1 (one) for hexagons with a probability of 0 for the period 1950–2020 but with previous affectations (1851–1950), indicating that the H hazard is not null in the area.

3.2 Vulnerability index

This study used census datasets for years 2000, 2010, and 2020 from the National Institute of Statistics and Geography (INEGI 2001, 2011, 2021). The selected analysis unit was the locality as a point reported in the main results by locality (ITER), corresponding to the higher-resolution spatial unit for which socioeconomic data are available. We used 310, 315, and 316 ITERs for vulnerability and exposure calculations corresponding to 2000, 2010, and 2020, respectively. The changes documented in the ITER administrative boundaries did not affect the analysis because socioeconomic data were integrated into the hexagonal grids created previously. For rural areas, we assigned ITER point values to the spatially corresponding hexagon; for urban areas, we assigned the data from the urban polygons established by INEGI. As the hexagonal grid intersected these polygons, socioeconomic data were partitioned among the hexagons proportionally to the area included in each.

The first step in the vulnerability analysis was the selection of variables related to this risk component. Given the changes in the parameters collected in each census, we limited the number of variables considered. We collected an initial set of 19 indicators based on previous research (Cutter et al. 2003; Siagian et al. 2014; León-Cruz and Castillo-Aja 2022), but only 15 were maintained after the correlation analysis (Table 1). The resulting variables represent social, economic, and structural characteristics related to vulnerability. Then, each variable was standardised by converting the values to z-scores for comparison purposes.

With the selected variables, factor analyses were performed. This multivariate statistical method has been widely used for developing vulnerability indices (e.g. Cutter et al. 2003; Siagian et al. 2014; Guillard-Gonçalves et al. 2015; de Loyola Hummell et al. 2016; Frigerio et al. 2018). This method reduces the number of variables related to vulnerability and facilitates the generation of weighted and unweighted indices. Factor analysis uses the principal components technique to calculate the initial factor loadings. Furthermore, varimax rotation and Kaiser normalisation were selected for data analysis (Siagian et al. 2014; Frigerio et al. 2016). It is worth noting that the Kaiser–Meyer–Olkin (KMO) and Bartlett's tests were performed. The KMO values obtained were 0.83, 0.76, and 0.77 for years 2000, 2010, and 2020, respectively, while Bartlett's test returned a p value lower than 0.001 in all cases. Such results confirm the applicability of the factor analysis.

Table 1 Variables used for the Social Vulnerability Index derived from 2000, 2010, and 2020 census datasets

ID	Description	Impact
PFEM	Percentage of female population	+
P5YM	Percentage of young children (under 5 years of age)	+
PSIND	Percentage of the population with no health services	+
PDISC	Percentage of disabled population	+
PANAL	Percentage of illiterate population	+
PESUP	Percentage of the population with tertiary education	–
PLIND	Percentage of indigenous population	+
PINAC	Percentage of economically inactive population	+
VPTIE	Percentage of households with dirt floors	+
VICUA	Percentage of households with a single room	+
VSAGU	Percentage of households with no drinking water	+
VSELE	Percentage of households with no electricity	+
VSRAD	Percentage of households with no radio	+
VSNTV	Percentage of households with no TV	+
VSAUT	Percentage of households with no motor vehicle	+

According to the scree plot and the Kaiser criterion, factors with an eigenvalue greater than one were extracted (Fig. 2). A total of four factors were derived that explained 73.0, 68.4, and 66.5% of the variance for 2000, 2010, and 2020, respectively. The resulting factors were labelled for each year, as shown in Table 2. In this table, health is the percentage of the population with no health services; education includes the portion of illiterate people, as well as those with tertiary education; poverty comprises the percentage of households with no radio, TV, or motor vehicle; gender represents the percentage of women in the general population; employment is the percentage of the economically inactive population; ethnicity is the proportion of indigenous people; marginalisation includes the percentage of households with dirt floors or lacking drinking water or electricity; age is the percentage of the population under five years old; and disability is the proportion of the population with any mobility or mental restrictions.

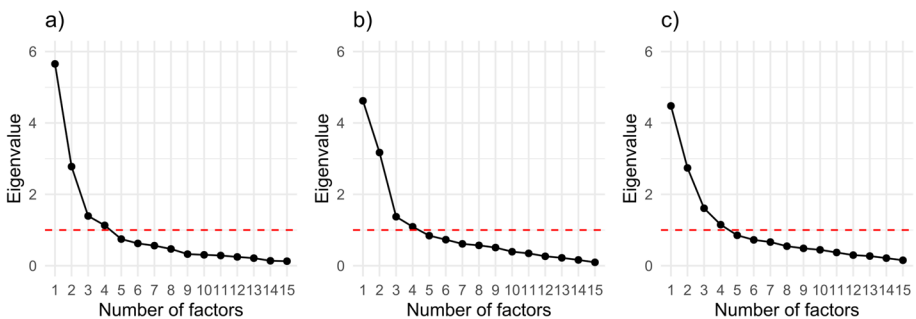


Fig. 2 Scree plot of the factor analyses for data corresponding to years (a) 2000, (b) 2010, and (c) 2020. Points above the red dashed line indicate eigenvalues greater than one

Table 2 Comparison of vulnerability index components for 2000, 2010, and 2020 census datasets

Year	ID	Component name	Variance
2000	F1	Health, education, and poverty	32.0%
	F2	Gender and employment	15.2%
	F3	Ethnicity and marginalisation	14.5%
	F4	Age and disability	11.3%
	Total variance explained		73.0%
2010	F1	Gender and marginalisation	29.1%
	F2	Education and ethnicity	18.5%
	F3	Poverty	12.0%
	F4	Disability	8.8%
	Total variance explained		68.4%
2020	F1	Gender and marginalisation	25.9%
	F2	Age and education	16.3%
	F3	Ethnicity and poverty	16.1%
	F4	Disability	8.2%
	Total variance explained		66.5%

It is important to note that there are standard dominant components in the three years analysed, a situation reported previously (Zhou et al. 2014). From these results, three vulnerability indices were developed. To this end, an approach based on unequal weighted scoring was used (Siagian et al. 2014; Frigerio et al. 2016). The final scores were constructed using the approach proposed by Siagian et al. (2014) (Eq. 2).

$$SVI_y = \sum_{i=0}^n \frac{F_n \times V_n}{V_t} \quad (2)$$

where SVI_y is the social vulnerability index for the year analysed (y), F_n represents the factors collected each year, V_n denotes the per cent variance explained by each factor, and V_t is the total explained variance. The resulting values of each vulnerability index were reclassified using the standard deviation classification method, as suggested in previous research (e.g. Siagian et al. 2014).

3.3 Exposure index

As in previous studies, exposure to Hs was calculated using the population density approach (León-Cruz and Castillo-Aja 2022). The population density in each hexagonal grid cell in the study area was calculated with the same data sources and spatial unit used for the SVI. It is worth mentioning that the total area of each grid cell was estimated excluding water bodies (e.g. lakes, coastal lagoons) because of the significant impact of these areas on the distribution of populations. Then, a logarithmic function was applied following previous methodologies to reduce the effects of the main population centres (e.g. Mérida, Yucatan, or Benito Juárez, Quintana Roo). The exposure index for each year (EI_y) was computed using the approach proposed by CENAPRED (2006) (Eq. 3). The resulting values were then reclassified using the natural breaks (Jenks) classification method.

$$EI_y = \log(PD_y) + 3 \quad (3)$$

where PD_y is the population density calculated for each year in each hexagonal cell.

3.4 Risk index

Based on the three risk components and periods explained above, we developed nine indices to approach the hurricane-force wind risk assessment in the Yucatan Peninsula. To this end, we used each H risk component, i.e. hazard, vulnerability, and exposure (for 2000, 2010, and 2020), to construct a 3D-risk matrix based on the concept proposed by Kamranzad et al. (2020). The hurricane-force wind risk index (*HRI*) for each year was calculated according to the following equation (Eq. 4):

$$HRI_y = HI_y \times SVI_y \times EI_y \quad (4)$$

where HI_y , SVI_y , and EI_y represent the hazard, vulnerability, and exposure indices, respectively, for each year (y). Based on these results, we reclassified *HRI* values by calculating the quintiles from the non-null 3-time period dataset and, consequently, assigned five risk levels in addition to the null level. Finally, we computed the changes in H risk using the differences between the periods analysed.

4 Results and discussion

4.1 Hazard

The annual probabilities of hurricane-force wind occurrence ranged from 0 to 0.111 for the period 1950–2000, from 0 to 0.137 for 1950–2010, and from 0 to 0.144 for 1950–2020. Cozumel Island exhibited the highest probabilities for the three periods (Fig. 3). However, values above 0.1 were computed for the island for the year 2000, in contrast with 2010 and, particularly, 2020, when large areas of northern Quintana Roo and the east of the Yucatan state presented this range of data. On the contrary, probabilities tend to decrease over time in the southeast. This result is consistent with the trends detected for major Hs (3+ on the Saffir–Simpson scale) in the area by Martinez et al. (2023). These authors measured a decrease in the frequency of major Hs in southern Quintana Roo and an increase to the north.

For each year, values greater than 0.05 were found in three parallel strips with a southeast-to-northwest orientation (Fig. 3). The largest strip extends from the southern region of Quintana Roo from the Cozumel-Riviera Maya region to the central-north Yucatán coast; the second strip encompasses most of central Quintana Roo; and the third, i.e. the narrowest strip, is located in southern Quintana Roo. These three zones correspond to typical H trajectories in the area (NHC Tropical Cyclone Climatology <https://www.nhc.noaa.gov/climo/>). Most landfalling Hs have entered the Riviera Maya zone and penetrated across the peninsula to reach northern Yucatan, as was the case of TCs “Zetta” and “Gamma” in 2020. Also, the high probabilities in the north are related to multiple TCs that circulated through the Yucatan Channel, such as “Ida” in 2009. Other TCs that made landfall on the central Quintana Roo Caribbean coast early in the TC season, then travelling to the Yucatan–Campeche border in the Gulf of Mexico

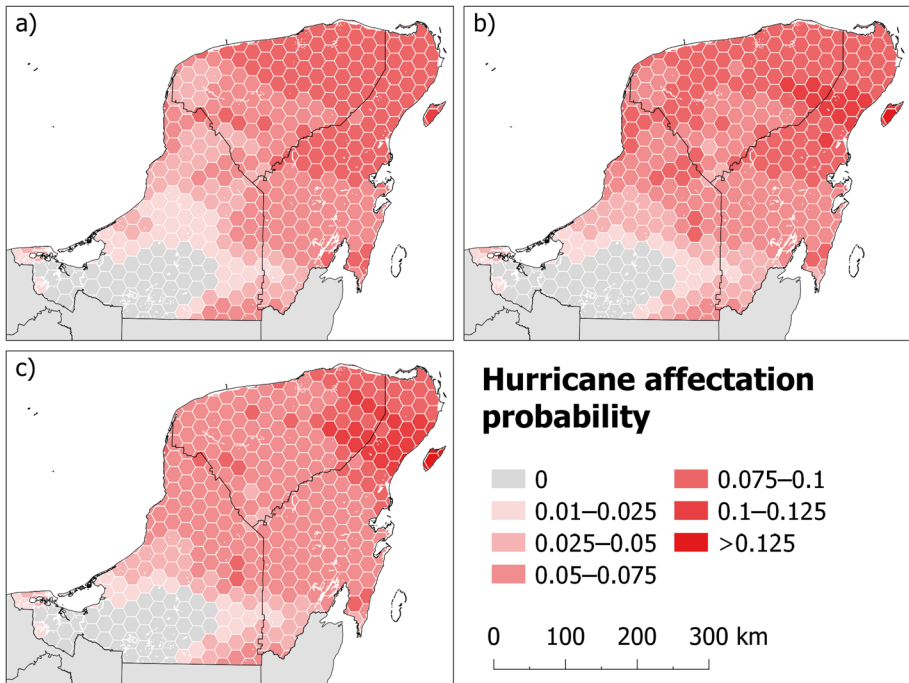


Fig. 3 Spatial distribution of the annual probability of hurricane affection for years (a) 2000, (b) 2010, and (c) 2020

coastal zone, were "Hilda" in 1955 and "Stan" in 2005". Finally, many early-season TCs made landfall near Chetumal, coming out considerably weakened in southern/central Campeche early in the season, like "Alex" in 2010.

Regarding areas with low probability of impact, the southern zone of the study area showed a null probability of affection in the period 1950–2000. However, when data for subsequent decades were included, only southwestern Campeche maintained a null probability of affection for all periods, which included the general calculations derived from the complete IBTrACS database (1851–2022). These results demonstrate the difficulty of evaluating the spatiotemporal evolution of hazards from data spanning short periods due to the rare occurrence of tropical cyclones. This null-hazard area is protected since tropical cyclones circulate from east to west or from north to south; therefore, the systems that may affect the southwest Campeche are always markedly weakened. The area with no records (i.e. the unaffected area) is relatively small, showing the deep inland penetration of cyclonic systems after making landfall. The circulation of the systems towards the northwest prevents frequent H affection in southern and western Campeche, with annual probabilities lower than 0.02 (Fig. 3).

On the hazard map (Fig. 4), the highest probabilities of H wind affection translate into large zones with high and very high *HI* values, while the null-hazard area is spatially limited. Indeed, the use of H trajectories for 1851–1950, despite underestimating H frequencies due to the lack of reliable records, allowed us to reduce the zone with a null probability of affection, equivalent to an *HI* value of zero. In 2000, the highest *HI* value corresponded to a high hazard observed on Cozumel Island and the mainland

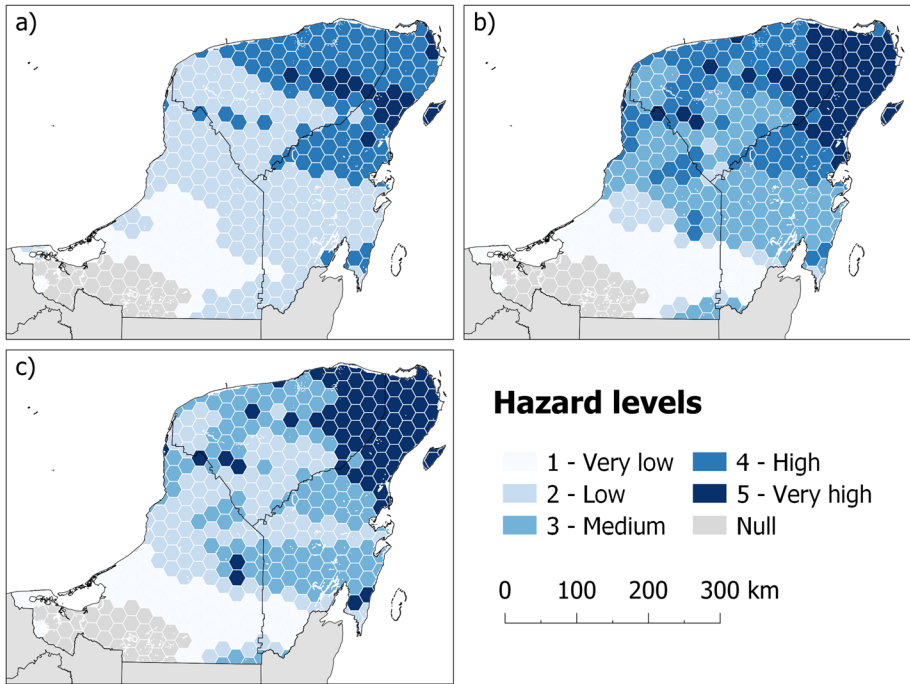


Fig. 4 Spatial distribution of hurricane hazard levels for years (a) 2000, (b) 2010, and (c) 2020

along a strip from Playa del Carmen to central Yucatan. Another zone with a very high *HI* extended between Cancún and Cabo Catoche. In 2010, a very high hazard level was identified in the same locations, although with a wider geographic reach, encompassing the entire northern region of Quintana Roo. In 2020, a zone of very high hazard comprised an even larger region that stretched to the west. Also, very high *HI* hexagons were observed in the south of the study area. The northeast of the peninsula and southern Quintana Roo were affected by hurricanes during 2011–2020, indicating the gradual expansion of the area with very high *HI* over time. However, this also reduced the prevalence of high *HI* values between 2000 and 2010 or 2020. This trend indicates a concentration of high-risk zones in the northeast region. Pooling together the high and very high *HI* categories revealed that 2010 recorded the most significant expansion.

The gradual increase in *HI* between 2000 and 2020 may be related to climate change, which can affect *Hs* in several ways (Murakami et al. 2020). Moreover, most models showed that the climate promoted a slight increase in hurricane wind intensity. Some scientists believe that climate change associated with human activities promoted increased *H* frequency and intensity (Knutson et al. 2015) in the Atlantic basin. The 1970s corresponded to a cold phase in Atlantic Ocean surface temperature (Terry 2012), which did not favour the formation of TCs (Goldenberg et al. 2001) and may have influenced the hazard level for the period 1950–2000, as this colder period represent a greater proportion of the time interval used for calculating hazard probabilities than it did for 2010 or 2020.

4.2 Vulnerability

Maps of hurricane vulnerability levels in Mexico were constructed based on the statistical analysis and the calculated weighted indices (Fig. 5). As mentioned above, the vulnerability index for each year was estimated from four factors. The extracted components and their respective explained variance are shown in Table 2.

In the three years analysed, four main components were related to the vulnerability to hurricanes. Still, the explained variances for each component reduced their differences over time. For example, the explained variances for the first and fourth components in the year 2000 were 32% and 11.3%, equivalent to a 20.7% difference, which is higher than the differences between the first and fourth components in 2010 (20.3%) and 2020 (17.7%). This can be interpreted as a levelling trend among the central components of vulnerability, that is, the weight of each component tended to level off over time. For this reason, the use of weighted indices different from the original SoVI methodology proposed by Cutter et al. (2003) was crucial. Similar studies (e.g. Zhou et al. 2014) have also reported a similar behaviour. In this same matter, the decreasing trend in the total explained variance from 73% in 2000 to 66.5% in 2020 can be interpreted as resulting from emergent factors related to vulnerability, which, given the nature of this statistical approach, were not considered (i.e. because of the use of factors with an eigenvalue greater than one) in the indices, mainly in years 2010 and 2020.

Another interesting feature is the presence of common vulnerability drivers in the three years analysed. For example, gender is present as F2 (2000), F1 (2010), and F1 (2020);

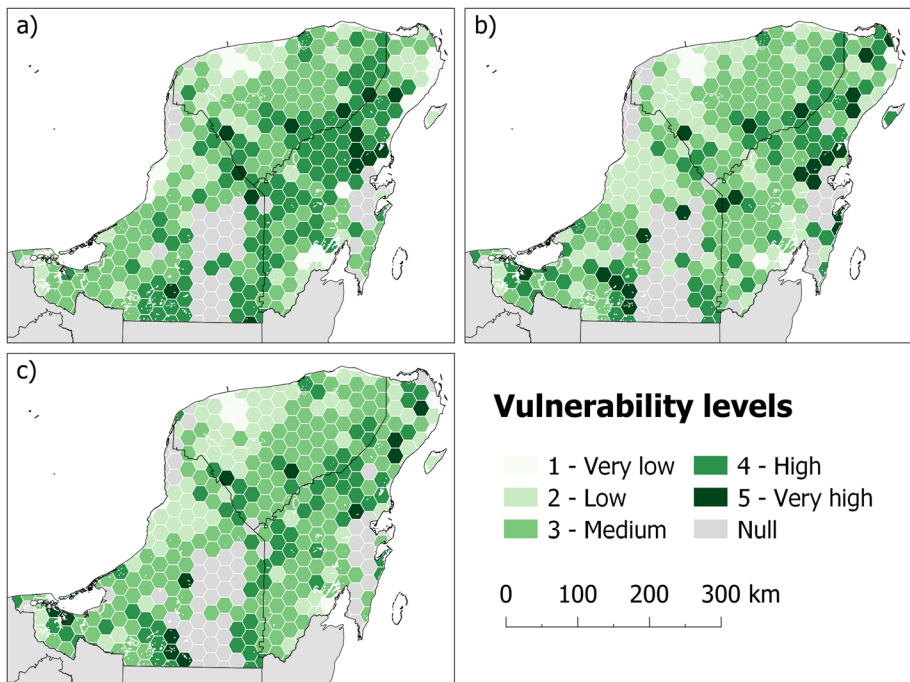


Fig. 5 Spatial distribution of vulnerability levels for years (a) 2000, (b) 2010, and (c) 2020

marginalisation as F3 (2020), F1 (2010), and F1 (2020); education as F1 (2000), F2 (2010), and F2 (2020); and poverty as F1 (2000), F3 (2010), and F3 (2020). The above suggests that these components are the most important and constant characteristics of the population in the study area that have increased their propensity to suffer damage from the impact of Hs. Other investigations have mentioned the central role of similar elements in the vulnerability to natural hazards (e.g. Cutter et al. 2003; Zhou et al. 2014; León-Cruz and Castillo-Aja 2022).

Marginalisation is related to socioeconomic deprivation or exclusion. At the same time, poverty refers to low income that leads to under-consumption. The literature has previously discussed the relationship between vulnerability, marginalisation, and poverty (e.g. Cardona 2011; Martínez-Martínez and Rodríguez-Brito 2020; Tenzing 2020). In the YP, poverty has been historically related to indigenous populations, specifically the Maya. Previous research has also noted that marginalisation in the YP has remained very high over the past decades, making little progress or remaining static compared to the national trends (Ramírez-Carrillo 2020). In this context, the results of this research confirmed the existence of root causes leading to poverty and marginalisation in specific groups (i.e. indigenous populations) in the YP that adversely affect vulnerability, as observed at the country level (León-Cruz and Castillo-Aja 2022). Notably, the above is observed in some areas of the YP despite their apparent vigorous economic development, as discussed below.

According to raw data from INEGI, the percentages of illiterate and higher-education populations show contrasting behaviours in the study area, that is, a decreasing trend in the former (22, 16.3, and 11.8% for years 2000, 2010, and 2020), and an increasing trend in the latter (5, 13.8, and 22.1% for 2000, 2010, and 2020). Access to higher education combined with the decrease in illiteracy should be a potential factor to reduce vulnerability; however, this was not observed in the study area. Spatially, there was a reduction in areas with education issues; however, these issues are concentrated in zones that are important enough to indicate education as a key driver of vulnerability in the study area. Previous studies have mentioned that the greatest educational backlog in the Yucatan Peninsula is concentrated mainly in rural, highly marginalised areas inhabited by indigenous communities (Camargo Medina 2022). Some regions of the YP (including those mentioned above) have not experienced significant advances in educational parameters in the past 20 years, which has led to substantial impacts on vulnerability to natural hazards such as hurricanes.

In this research, the gender component refers to the female population. Some studies have identified the forms of inequality associated with women that affect their vulnerability; for example, women are considered less able to make decisions, have less access to resources, and earn lower salaries (Soares et al. 2014). In the analysed area, we noted two situations that highlight these aspects. First, there is an increasing percentage of women in the population (from 46.6% in 2000 to 48% in 2020), which may influence the vulnerability in the region. Second, and more importantly, there are gender-related forms of inequality in the YP not addressed yet that can be considered the root causes of this vulnerability. It should be noted that both factors, i.e. education and gender, have been identified as central drivers of vulnerability in Mexico (e.g. Bell et al. 2008; Gran Castro and Ramos De Robles 2019; Mirinda and Lazos Chavero 2022).

As regards the disability component, its occurrence in the last position (F3) in the three years analysed is also interesting. The percentage of the population with any disability has been on the rise in recent years, from 2.0% in 2000 to 5.4% in 2020, according to the raw data from INEGI. Since this variable includes physical mobility, it can be associated with the ageing population living in the area. Mobility constraints are key drivers of vulnerability to Hs, particularly during emergencies, as they affect the ability of this population

group to take precautions quickly. Other authors (Pérez and Valdés 2021) have noted how the coexistence of elderly and disabled populations increases vulnerability. In addition, hyper-aged municipalities in some portions of the YP reflect severe deprivation associated with poverty, which affects these population groups to a greater extent.

The similarities between the distribution of factors in 2010 and 2020 can be associated with the socioeconomic conditions in the region (from which SVIs are calculated) that have not changed significantly in recent years. The latter differs from those observed between 2000 and 2020, showing a considerable difference in the parameters from which the hazard components were derived. Such differences can be linked to profound changes in the socioeconomic structure in the study area. Previous research has documented how critical changes, mainly related to the effects of the North American Free Trade Agreement (NAFTA), have driven economic growth in this part of the country (Ramírez-Carrillo 2020). Likewise, although migration was not considered an important factor related to vulnerability in the study area, previous studies mention how the YP has experienced immigration in recent years, mainly from rural to urban areas (Carte et al. 2010). In summary, although these factors have not markedly reduced vulnerability in the area, they have produced changes in its driving factors.

Spatial variations in vulnerability also provided valuable information (Fig. 5). The number of spatial units with high and very high vulnerability levels has decreased over time. Higher economic development and tourism levels have probably played a major role in the decrease in vulnerability observed. The above was most evident in the northern area of Quintana Roo. In the Yucatan state, the regions surrounding Mérida, the capital city, showed the lowest vulnerability levels in the years studied (and over the entire study area). The greatest changes in vulnerability in Yucatan were observed along the border with Quintana Roo in the southeast. On the other hand, an increased number of spatial units with high and very high vulnerability levels is observed in Campeche, mainly to the south of the state, along the border with Guatemala.

In particular, the increased activity in the tourism and services sectors reported previously in the YP (e.g. Sánchez Triana et al. 2016; Metcalfe et al. 2020) has led to a reduction in the number of spatial units with high and very high vulnerability levels in the present analysis because vulnerability was calculated based on social and economic characteristics, one of the most common approaches. However, future territorial transformations may lead to changes in ecosystem services and the potential reduction of natural barriers to strong winds associated with Hs in the study area. For example, the significant role of mangroves in buffering H-related storm surges and floods is well known (e.g. Sheng and Zou 2017). Our analyses showed that rural areas experienced the most substantial changes in vulnerability.

4.3 Exposure

The exposure levels calculated by population density are shown in Fig. 6. Exposure, like vulnerability, is considered a dynamic component within the risk analysis. In this sense, various studies point to the vital role of population growth in the increase in losses associated with the impact of natural phenomena and, thus, in the increasing number of disasters (e.g. Zhou et al. 2014; Zúñiga and Villoria 2018). Vigorous population growth is evident in the study area, mostly around the main population centres such as Mérida, Yucatan, and Cancún and Chetumal, Quintana Roo. Data from INEGI indicate that the total population size in the study area rose from 3 223 862 inhabitants in the year 2000 to 4,103,596 in

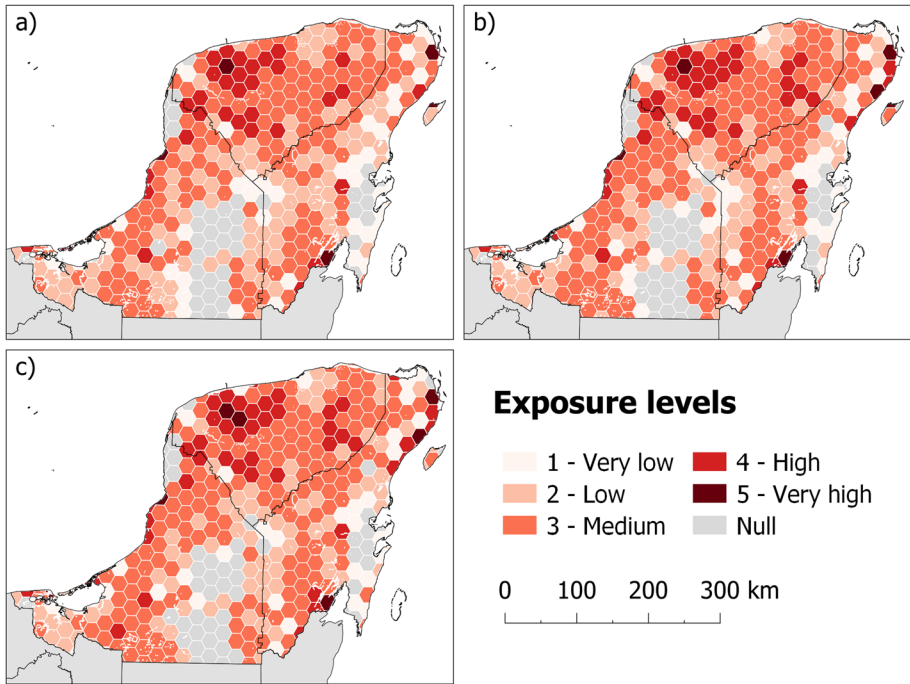


Fig. 6 Spatial distribution of exposure levels for years (a) 2000, (b) 2010, and (c) 2020

2010, and 5,107,246 in 2020. The population size increased in the three states; the most vigorous growth occurred in Quintana Roo, with nearly one million (983,022) additional inhabitants from 2000 to 2020.

The first key element observed is that large population centres display higher exposure levels in the three years considered. Interestingly, exposure calculations reveal the expansion of cities, such as Mérida, Yucatan, and tourism centres, such as Cancún, Quintana Roo. The larger number of inhabitants and the urban infrastructure have led to a growing number of elements exposed to natural hazards such as Hs. Other regions, mainly in the southern portion of the study area, show no major changes other than the increased exposure pattern. This south-to-north migration may be associated with economic development driven by tourism. It is worth noting that unpopulated areas covered mainly by tropical forests represent spatial units with null exposure values.

4.4 Risk

Risk levels reflect the combination of vulnerability, hazard, and exposure, revealing the areas where large populations are vulnerable to relatively frequent threats. The maps representing *HRI* levels (Fig. 7) highlight critical areas in the YP, mainly in Quintana Roo and eastern Yucatan. Although the highest *HRI* levels were found in northeast YP (Fig. 7), some very high *HRI* values related to medium- to very high-hazard and vulnerability levels were also obtained in the south in the year 2000—specifically, in the Mahahual hexagon—and in the south and northwest in 2010 and 2020, mainly in inland

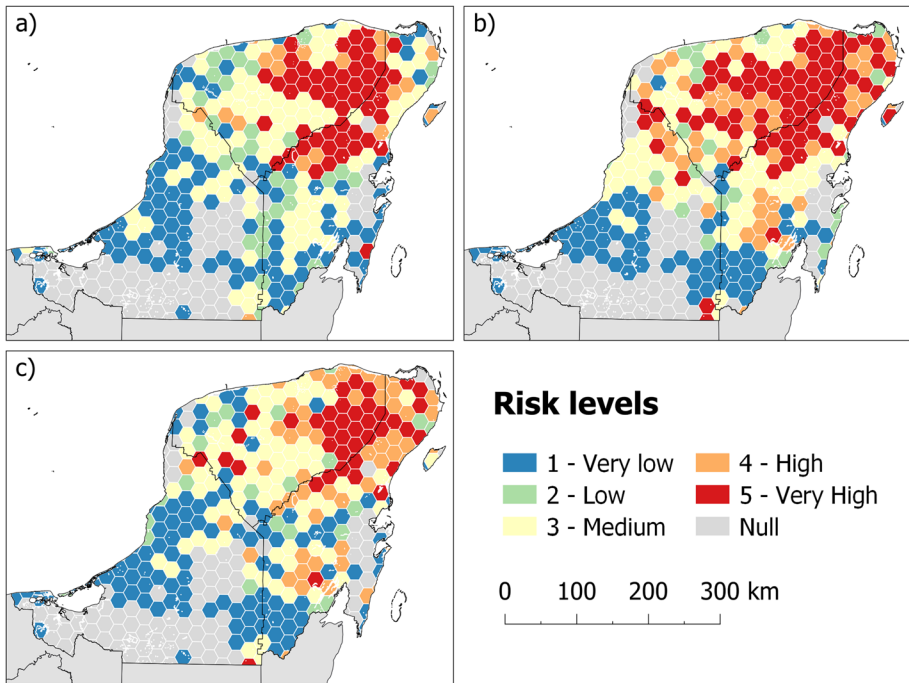


Fig. 7 Spatial distribution of hurricane risk levels for years (a) 2000, (b) 2010, and (c) 2020

areas. Particularly, a very high-risk level is appreciated in the eastern region of Yucatan in the three years, encompassing the most densely populated rural area associated with significant danger and high vulnerability. On the other hand, coastal urban areas such as Cozumel and the Riviera Maya, for which *HI* is greater and exposure is maximal (Fig. 5), produced moderate risk values due to their lower vulnerability (Fig. 4). Indeed, the Riviera Maya showed low- to medium-risk levels in the year 2000. By 2010 and 2020, the combination of a higher frequency of Hs (Figs. 3 and 4) and a higher population density due to immigration of workers led to increased risk levels locally.

Most hexagons with low *HRI* values are located in the southern half of the study area in the year 2000. In 2010, this sector became smaller, located in more southern zones where these hexagons were concentrated. Only in the area bordering Belize, hexagons in Campeche showed a high *HRI* in 2010, probably related to H landfalls in the neighbouring country. In particular, in the years 2000 and 2020 in the coastal region of southern Quintana Roo, the Mahahual hexagon stood out with high to very high *HRI* values in null-risk areas. In fact, from the *HI* and *EI* maps, the areas that show a null hazard or population also have a null risk. This level of analysis was possible due to the spatial units selected, which differ significantly from those used by the Mexican government in its National Risk Atlas (CENAPRED 2015). The number of hexagons with high- or very high-risk levels increased dramatically from 2000 to 2010, while the number of hexagons with low or very low levels decreased; this shift was slightly inverted between 2010 and 2020. In the trend analysis process, it is necessary to remember that the hazard and exposure indices were elaborated from the time series, thus assuming continuity.

The cold phase in the Atlantic skews the hazard during the 1970s (Goldenberg et al. 2001; NOAA 2019). Likewise, the population of the Yucatan Peninsula has grown continuously, resulting in higher levels of exposure. Finally, it should be noted that these hazard indices, and consequently the risk, are derived from the spatial analysis of H wind fields. However, despite being a key element of TC, the occurrence of hurricane-force winds is not the only significant factor in terms of destructive capacity. For example, the volume of rainfall that depends more on the displacement velocity, the size of the system, its wind history before arrival, and the underlying topography (Touma et al. 2019) can cause economic losses outside high-wind zones (Xi et al. 2020); these elements were not included in the present risk characterisation.

When comparing the *HRI* maps for 2010 and 2000 (Fig. 8a), it is evident that most changes are mainly associated with an increase in the *HI* (Fig. 4), resulting in the expansion of very high-, high-, and medium-level hazards throughout the YP. Most negative *HI* changes are located in the southern regions of Quintana Roo and Campeche, generally ranging from -1 to -2 . These can be attributed to a decrease in *HI* levels. In particular, the Mahahual hexagon experienced a -3 decrease in risk between the years 2000 and 2010, primarily due to a decrease in vulnerability. The negative variations in the northern half of the peninsula, evident as isolated hexagons, are due to a reduction in vulnerability.

An aspect worth noting is that the differences between 2020 and 2010 yielded more homogeneous results (Fig. 8b), revealing three identifiable sectors. First, a marked reduction in risk was observed in the northern half of the YP, with variations ranging from -3 to -1 . In general, these reductions are attributed to a decrease in *HI* during the study period;

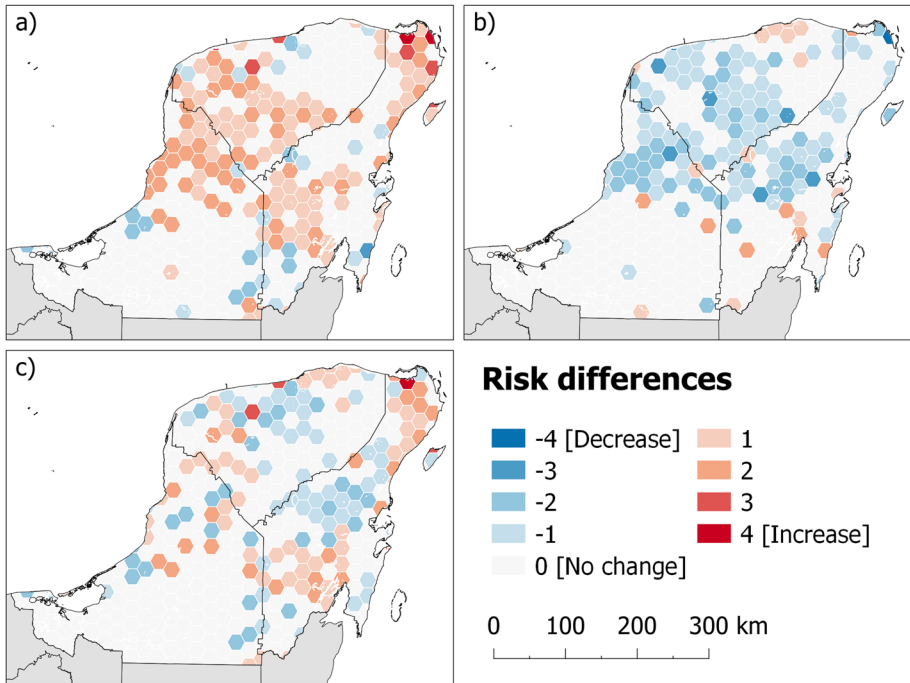


Fig. 8 Spatial distribution of the differences in hurricane risk for the periods (a) 2010–2000, (b) 2020–2010, and (c) 2020–2000

when the difference is -1 , the hazard decreases and, for higher differences, the reduction in hazard is associated with a decrease in vulnerability. Furthermore, a hexagon with a value of -4 was identified in north Quintana Roo; however, this value is not significant. In fact, the low population data for the 2020 ITER did not allow us to calculate vulnerability, artificially reducing the risk for this year.

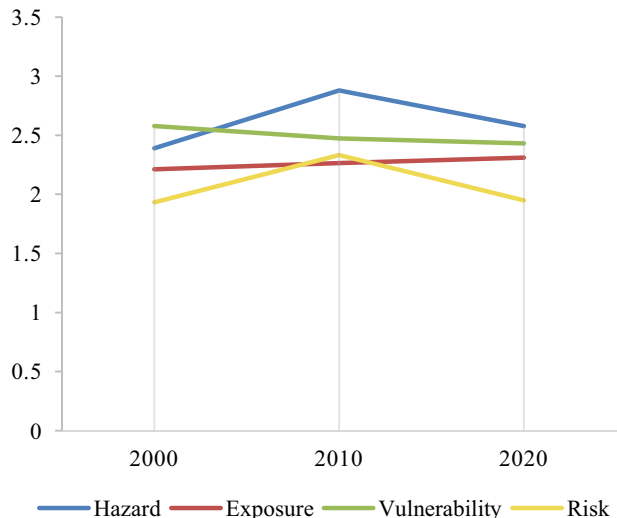
Second, northeast Yucatan showed a sector with a value of $+1$, linked to the expansion of the very high *HI* zone in the region due to frequent hurricane trajectories in the area. The third case is similar; values of $+1$ to $+2$ are found in the southern area, associated with the impacts of hurricanes passing between 2010 and 2020.

As a result, the overall evolution of risk for the period studied, from the difference between the years 2020 and 2000 (Fig. 8c), is spatially heterogeneous, with changes in *HI* ranging between -2 and $+4$. Risk reductions are observed mainly in the central areas of Yucatan and Quintana Roo, while increases appear in the northeast zone of the peninsula: the Riviera Maya and adjacent areas and northeast Yucatan. Less intense increases also affected south Quintana Roo, except for coastal areas ($+1$ to $+2$). In the northwest of the YP, the variation exhibited less regional disparity, with scattered hexagons indicating both positive and negative changes (-2 to $+3$).

Hazard evolution is the main driver of risk in the YP, as illustrated by the parallel curves of the spatial average of risk and hazard indices in Fig. 9. Therefore, as the Atlantic cold phase may have played a role in the low frequency of *Hs* during the 1970s (Goldenberg et al. 2001; NOAA 2019), it is essential to consider the potential bias of using this period as a baseline. Evidence of this potential bias is the lesser difference in hazard between 2020 and 2010 compared to the difference between 2010 and 2000 (Figs. 9 and 10). The peak hazard in 2010 can be confirmed by the fact that the decade from 2001 to 2010 had the highest occurrence of hurricanes in the North Atlantic throughout the entire database time span (Sánchez-Rivera et al. 2021).

Concerning the sociodemographic components, exposure continuously increased in the YP (Figs. 9 and 10); this is particularly important in touristic zones (e.g. Cancún, Tulum, Cozumel) such as the coastal areas of Quintana Roo (Fig. 6). Vulnerability is the only component that showed a decreasing index value during the study period due to economic growth, mainly

Fig. 9 Spatial average of the risk index and its components



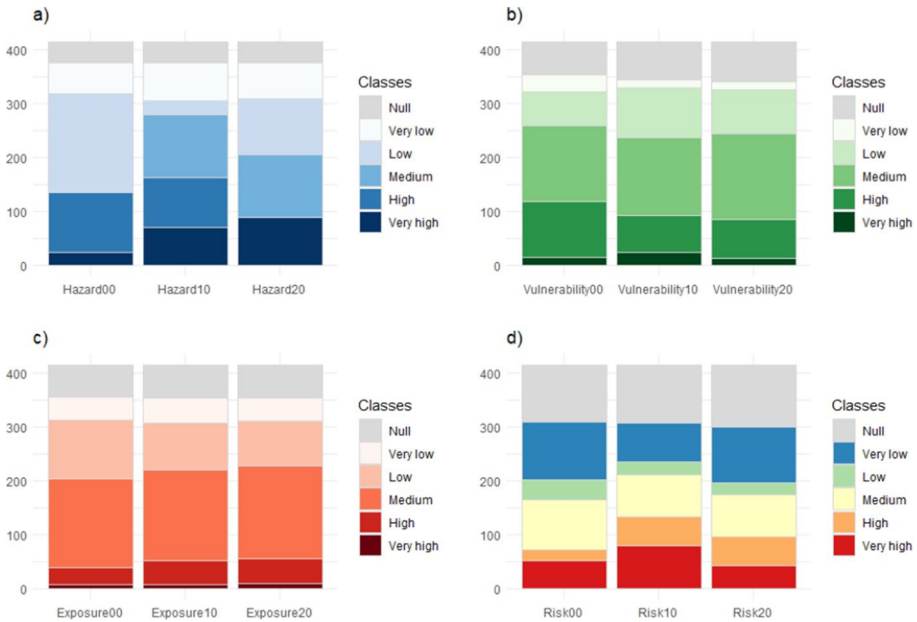


Fig. 10 Number of spatial units per (a) hazard, (b) vulnerability, (c) exposure, and (d) risk levels for years 2000, 2010, and 2020

driven by tourism (García de Fuentes et al. 2019) and public policies to reduce poverty (Pérez Medina 2011). However, the spatial average of the vulnerability index remains high relative to the other components due to the extension of poor rural areas (Zamudio-Sánchez et al. 2012).

It is also noteworthy that the average risk value is lower, particularly for 2020, relative to its components. This can be attributed to the fact that areas with a higher probability of impact, located along the Caribbean coast, have experienced a substantial reduction in vulnerability through the conversion from rural to urban or peri-urban zones. However, continuous population growth can significantly increase exposure along the entire coast, as is now the case in Cancún or Playa del Carmen, leading to a new increase in risk.

The increase in risk between 2000 and 2020 is relative, as illustrated in Fig. 8. The average value for both years is similar because, although there was an increase in high-risk areas, the number of very high-risk hexagons was minimal in 2020 (Fig. 10). Also, the number of cells with null risk and vulnerability increased between 2000 and 2020. Exposure also showed this variation, although to a lesser extent. This highlights a limitation of the present study: null vulnerability and, therefore, zero risk is assigned to cells with population numbers too low for the vulnerability calculation. We found four hexagons showing this problem and considered that having those few cases is better than underestimating vulnerability for the entire study area. Furthermore, this finding illustrates the dynamics of the rural exodus and an actual decrease in risk in these areas.

5 Conclusions

The present study evaluated the spatial and temporal changes in risk associated with hurricanes in the YP. To this end, we calculated the hazard, vulnerability, and exposure components of risk based on several datasets using a number of methodologies. Hazard was evaluated using the probabilities of occurrence of hurricane-force winds. Vulnerability was assessed by applying a multivariate statistical method and socioeconomic variables. Finally, exposure was defined by the change in population density. All the parameters mentioned above were computed for a hexagonal grid, different from several approaches that use municipalities as spatial units, which is not always helpful, especially in local and regional studies.

The resulting values in the indices show an increased risk in the study area, mainly in the northeast region. Such increases are driven primarily by the increased hazard and exposure to hurricanes. The increase in the first component is particularly relevant under a warming climate scenario and contributes to explaining the increased risk to Hs in the YP. It is impossible to attribute the rise in hazard to climate change, as the period with reliable data is too narrow to analyse trends at this spatial scale. Additionally, we acknowledge that the cold phase of the AMO in the 1970s resulted in abnormally low probabilities for the year 2000. Nevertheless, it is undeniable that global warming has led to warmer ocean water and changes in atmospheric conditions that have led to increased tropical cyclones (Camargo et al. 2023). Regarding exposure, the expansion of urban areas and the growing development of tourism are two major drivers. As a result, more people are settling in vulnerable areas, increasing the potential for loss of life and property damage from severe weather events.

The Riviera Maya region (north of the study area) is a prime example of the complex interaction between population growth, climate change, and economic development (García de Fuentes et al. 2019), contributing to increased risk related to hurricanes. Moreover, the appeal created by the Riviera Maya has spurred a demographic dynamic in the nearby continental zones, increasing exposure with a persistently high vulnerability that together leads to increased risk in the northeast of the YP. Therefore, it is essential to implement comprehensive risk management strategies that address these unique challenges to ensure the safety and sustainability of communities and the economy in this region.

Despite this research showing a multiannual hurricane-force wind risk assessment, we have identified several limitations. For the hazard component, several threats, such as precipitation and storm surges, have not been considered directly as in other studies (e.g. Boragapu et al. 2023). The above is critical, especially for the impacts on flood risk. Future studies should focus on these particular threats related to hurricanes. On the other hand, we computed vulnerability indices using a limited set of socioeconomic data.

Despite these limitations, the results reported here help identify priority regions prone to hurricane impacts on the Yucatan Peninsula. In addition, this is the first research of its type in Mexico, which could set the basis for future studies at regional or national levels for other types of natural hazards. Finally, increasing understanding of risk-driven factors and their changes over time is the first step in improving disaster-reduction strategies at the local level.

Supplementary Information The online version contains supplementary material available at <https://doi.org/10.1007/s11069-023-06397-w>.

Acknowledgements This work was supported by the “Programa de Apoyo a Proyectos de Investigación e Innovación Tecnológica (PAPIIT)” of the UNAM [grant number IA101823].

Author's contributions DR and JFLC contributed to the conceptualisation; DR and JFLC were involved in the methodology; DR and JFLC assisted in the software; DR and JFLC contributed to the validation; DR and JFLC were involved in the formal analysis; DR and JFLC assisted in the investigation; DR contributed to the resources; DR assisted in the data curation; DR and JFLC contributed to the writing—original draft preparation; DR and JFLC were involved in the writing—review and editing; JFLC contributed to the visualisation; DR assisted in the supervision; DR was involved in the project administration; and DR contributed to the funding acquisition.

Funding This work was supported by the “Programa de Apoyo a Proyectos de Investigación e Innovación Tecnológica (PAPIIT)” of UNAM [grant number IA101823].

Data availability Data are available on the NOAA and INEGI web pages. <https://www.ncei.noaa.gov/data/international-best-track-archive-for-climate-stewardship-ibtracs/v04r00/access/shapefile/IBTrACS.NA.list.v04r00.points.zip> <https://www.inegi.org.mx/programas/ccpv/2020/> <https://www.inegi.org.mx/programas/ccpv/2010/>

Code availability The code applied was written in R, a programming language and free software environment for statistical computing and graphics supported by the R Foundation for Statistical Computing.

Declarations

Conflict of interest The authors declare that they have no conflict of interest. The funding entities did not play any role in the study design; data collection, analysis, or interpretation; manuscript writing, or in the decision to publish the results.

Open Access This article is licensed under a Creative Commons Attribution 4.0 International License, which permits use, sharing, adaptation, distribution and reproduction in any medium or format, as long as you give appropriate credit to the original author(s) and the source, provide a link to the Creative Commons licence, and indicate if changes were made. The images or other third party material in this article are included in the article's Creative Commons licence, unless indicated otherwise in a credit line to the material. If material is not included in the article's Creative Commons licence and your intended use is not permitted by statutory regulation or exceeds the permitted use, you will need to obtain permission directly from the copyright holder. To view a copy of this licence, visit <http://creativecommons.org/licenses/by/4.0/>.

References

- Accastello C, Cocuccioni S, Teich M (2021) The concept of risk and natural hazards. In: Protective Forests as Ecosystem-Based Solution for Disaster Risk Reduction (Eco-DRR)[Working Title]. IntechOpen AMIS (2021) De las diez catástrofes con más impacto al patrimonio de los mexicanos, cuatro son huracanes: AMIS. <https://sitio.amis.com.mx/de-las-diez-catastrofes-con-mas-impacto-al-patrimonio-de-los-mexicanos-cuatro-son-huracanes-amis/>. Accessed 10 Mar 2023
- Appendini CM, Meza-Padilla R, Abud-Russell S et al (2019) Effect of climate change over landfalling hurricanes in the Yucatan Peninsula. *Clim Change* 157:469–482. <https://doi.org/10.1007/s10584-019-02569-5>
- Bell ML, O'neill MS, Ranjit N et al (2008) Vulnerability to heat-related mortality in Latin America: a case-crossover study in Sao Paulo, Brazil, Santiago, Chile and Mexico City, Mexico. *Int J Epidemiol* 37:796–804
- Boose ER, Foster DR, Plotkin AB, Hall B (2003) Geographical and historical variation in hurricanes across the Yucatan Peninsula. *Lowl Maya Area Haworth N Y NY EEUU* 495–516
- Boragapu R, Guhathakurta P, Sreejith OP (2023) Tropical cyclone vulnerability assessment for India. *Nat Hazards* 117:3123–3143. <https://doi.org/10.1007/s11069-023-05980-5>
- Bronfman NC, Repetto PB, Guerrero N et al (2021) Temporal evolution in social vulnerability to natural hazards in Chile. *Nat Hazards* 107:1757–1784
- Camargo Medina JV (2022) Desigualdad y rezago educativo en la Península de Yucatán: 2015–2019. Master's Thesis, Universidad Autónoma del Estado de Quintana Roo

- Camargo SJ, Murakami H, Bloemendaal N et al (2023) An update on the influence of natural climate variability and anthropogenic climate change on tropical cyclones. *Trop Cyclone Res Rev*. <https://doi.org/10.1016/j.tcr.2023.10.001>
- Cardona OD (2011) Disaster risk and vulnerability: concepts and measurement of human and environmental insecurity. In: *Coping with global environmental change, disasters and security: threats, challenges, vulnerabilities and risks*. Springer, pp 107–121
- Carte L, McWatters M, Daley E, Torres R (2010) Experiencing agricultural failure: Internal migration, tourism and local perceptions of regional change in the Yucatan. *Geoforum* 41:700–710
- CENAPRED (2015) Grado de riesgo por ciclones tropicales
- CENAPRED (2006) Guía básica para la elaboración de atlas estatales y municipales de peligros y riesgos. Conceptos básicos sobre peligros, riesgos y su representación geográfica
- CRED (2022) EM-DAT The international disasters database of the Centre for Research on the Epidemiology of Disasters. <https://public.emdat.be/>. Accessed 10 Jan 2022
- Cutter SL, Boruff BJ, Shirley WL (2003) Social vulnerability to environmental hazards. *Soc Sci Q* 84:242–261
- Cutter SL, Finch C (2008) Temporal and spatial changes in social vulnerability to natural hazards. *Proc Natl Acad Sci* 105:2301–2306
- Dahal P, Shrestha NS, Shrestha ML et al (2016) Drought risk assessment in central Nepal: temporal and spatial analysis. *Nat Hazards* 80:1913–1932
- de Loyola Hummell BM, Cutter SL, Emrich CT (2016) Social vulnerability to natural hazards in Brazil. *Int J Disaster Risk Sci* 7:111–122
- Dominguez C, Magaña VO (2018) The role of tropical cyclones in precipitation over the tropical and subtropical North America. *Front Earth Sci* 6:19. <https://doi.org/10.3389/feart.2018.00019>
- Elsner JB, Hodges RE, Jagger TH (2012) Spatial grids for hurricane climate research. *Clim Dyn* 39:21–36. <https://doi.org/10.1007/s00382-011-1066-5>
- Elsner JB, Jagger TH (2013) *Hurricane climatology: a modern statistical guide using R*. Oxford University Press, USA
- Farfán LM, D'Sa EJ, Liu K, Rivera-Monroy VH (2014) Tropical cyclone impacts on Coastal Regions: the Case of the Yucatán and the Baja California Peninsulas, Mexico. *Estuaries Coasts* 37:1388–1402. <https://doi.org/10.1007/s12237-014-9797-2>
- Frigerio I, Carnelli F, Cabinio M, De Amicis M (2018) Spatiotemporal pattern of social vulnerability in Italy. *Int J Disaster Risk Sci* 9:249–262
- Frigerio I, Ventura S, Strigaro D et al (2016) A GIS-based approach to identify the spatial variability of social vulnerability to seismic hazard in Italy. *Appl Geogr* 74:12–22
- García de Fuentes A, Jouault S, Romero D (2019) Representaciones cartográficas de la turistificación de la península de Yucatán a medio siglo de la creación de Cancún. *Investig Geogr*. <https://doi.org/10.14350/ig.60023>
- García-Benítez M, Adame-Martínez S (2017) Propuesta metodológica para evaluar la vulnerabilidad por ciclones tropicales en ciudades expuestas. *Quivera Rev Estud Territ* 19:35–58
- García-Franco JL, Chadwick R, Gray LJ et al (2023) Revisiting mechanisms of the Mesoamerican Midsummer drought. *Clim Dyn* 60:549–569. <https://doi.org/10.1007/s00382-022-06338-6>
- Goldenberg SB, Landsea CW, Mestas-Núñez AM, Gray WM (2001) The recent increase in Atlantic hurricane activity: causes and implications. *Science* 293:474–479. <https://doi.org/10.1126/science.1060040>
- Gran Castro JA, Ramos De Robles SL (2019) Climate change and flood risk: vulnerability assessment in an urban poor community in Mexico. *Environ Urban* 31:75–92
- Guillard-Gonçalves C, Cutter SL, Emrich CT, Zêzere JL (2015) Application of Social Vulnerability Index (SoVI) and delineation of natural risk zones in Greater Lisbon, Portugal. *J Risk Res* 18:651–674
- Guzmán Noh G, Rodríguez Esteves JM (2016) Elementos de la vulnerabilidad ante huracanes. Impacto del huracán Isidoro en Chahihau, Yobaín, Yucatán. *Política Cult* 45:183–210
- Holland GJ (1980) An analytic model of the wind and pressure profiles in hurricanes. *Mon Weather Rev* 108:1212–1218. [https://doi.org/10.1175/1520-0493\(1980\)108<1212.CO;2](https://doi.org/10.1175/1520-0493(1980)108<1212.CO;2)
- Homewood P (2019) Tropical hurricanes in the age of global warming. The Global Warming Policy Foundation
- Horinouchi T, Shimada U, Wada A (2020) Convective bursts with gravity waves in tropical cyclones: case study with the Himawari-8 satellite and idealized numerical study. *Geophys Res Lett* 47:e2019GL086295. <https://doi.org/10.1029/2019GL086295>
- INEGI (2021) Censo de Población y Vivienda 2020. <https://www.inegi.org.mx/programas/ccpv/2020/>. Accessed 5 Jan 2023
- INEGI (2001) Censo de Población y Vivienda 2000. <https://www.inegi.org.mx/programas/ccpv/2000/>. Accessed 5 Jan 2023

- INEGI (2011) Censo de Población y Vivienda 2010. <https://www.inegi.org.mx/programas/ccpv/2010/>. Accessed 5 Jan 2023
- IPCC (2012) Managing the risks of extreme events and disasters to advance climate change adaptation: special report of the intergovernmental panel on climate change, [Field CB, Barros V, Stocker TF, Qin D, Dokken DJ, Ebi KL, Mastrandrea MD, Mach KJ, Plattner G-K, Allen SK, Tignor M, and Midgley PM (eds)]. Cambridge University Press. Cambridge University Press, Cambridge, United Kingdom and New York, NY, USA
- Kamranzad F, Memarian H, Zare M (2020) Earthquake risk assessment for Tehran. Iran ISPRS Int J Geo-Inf 9:430
- Knapp KR, Diamond HJ, Kossin JP, et al (2018) International Best Track Archive for Climate Stewardship (IBTrACS) Project, Version 4
- Knapp KR, Kruk MC, Levinson DH et al (2010) The international best track archive for climate stewardship (IBTrACS): unifying tropical cyclone data. Bull Am Meteorol Soc 91:363–376. <https://doi.org/10.1175/2009BAMS2755.1>
- Knutson TR, Sirutis JJ, Zhao M et al (2015) Global projections of intense tropical cyclone activity for the late twenty-first century from dynamical downscaling of CMIP5/RCP4.5 scenarios. J Clim 28:7203–7224. <https://doi.org/10.1175/JCLI-D-15-0129.1>
- Landsea CW, Franklin JL (2013) Atlantic hurricane database uncertainty and presentation of a new database format. Mon Weather Rev 141:3576–3592. <https://doi.org/10.1175/MWR-D-12-00254.1>
- Lawrence MB, Gross JM (1989) Atlantic hurricane season of 1988. Mon Weather Rev 117:2248–2259. [https://doi.org/10.1175/1520-0493\(1989\)117%3c2248:AHSO%3e2.0.CO;2](https://doi.org/10.1175/1520-0493(1989)117%3c2248:AHSO%3e2.0.CO;2)
- León-Cruz JF, Castillo-Aja R (2022) A GIS-based approach for tornado risk assessment in Mexico. Nat Hazards 114:1563–1583. <https://doi.org/10.1007/s11069-022-05438-0>
- Marín-Monroy EA, Hernández-Trejo V, Romero-Vadillo E, Ivanova-Boncheva A (2020) Vulnerability and risk factors due to Tropical cyclones in coastal cities of Baja California Sur, Mexico. Climate 8:144. <https://doi.org/10.3390/cli8120144>
- Martínez L-C, Romero D, Alfaro EJ (2023) Assessment of the spatial variation in the occurrence and intensity of major hurricanes in the Western Hemisphere. Climate 11:15. <https://doi.org/10.3390/cli11010015>
- Martínez-Martínez OA, Rodríguez-Brito A (2020) Vulnerability in health and social capital: a qualitative analysis by levels of marginalization in Mexico. Int J Equity Health 19:1–10
- Mendoza ET, Trejo-Rangel MA, Salles P et al (2013) Storm characterization and coastal hazards in the Yucatan Peninsula. J Coast Res 65:790–795. <https://doi.org/10.2112/SI65-134.1>
- Metcalfe SE, Schmook B, Boyd DS et al (2020) Community perception, adaptation and resilience to extreme weather in the Yucatan Peninsula, Mexico. Reg Environ Change. <https://doi.org/10.1007/s10113-020-01586-w>
- Mirenda C, Lazos Chavero E (2022) Cultural vulnerability, risk reduction and gender equity: two Mexican coastal communities. Environ Hazards 21:235–253
- Murakami H, Delworth TL, Cooke WF et al (2020) Detected climatic change in global distribution of tropical cyclones. Proc Natl Acad Sci U S A 117:10706–10714. <https://doi.org/10.1073/pnas.1922500117>
- Nederhoff K, Giardino A, Van Ormondt M, Vatvani D (2019) Estimates of tropical cyclone geometry parameters based on best-track data. Nat Hazards Earth Syst Sci 19:2359–2370. <https://doi.org/10.5194/nhess-19-2359-2019>
- Neumann CJ, Elms JD (1993) Tropical Cyclones of the North Atlantic Ocean, 1871–1992. National Climatic Data Center
- Nie C, Li H, Yang L et al (2012) Spatial and temporal changes in flooding and the affecting factors in China. Nat Hazards 61:425–439
- NOAA (2019) Atlantic high-activity eras: What does it mean for hurricane season? In: Natl. Ocean. Atmospheric Adm. <https://www.noaa.gov/stories/atlantic-high-activity-eras-what-does-it-mean-for-hurricane-season>. Accessed 5 Jan 2023
- Nordhaus W (2006) The economics of hurricanes in the United States. National Bureau of Economic Research, Cambridge, MA
- Pérez GC, Valdés GIV (2021) El envejecimiento poblacional a nivel municipal en Yucatán, evidencia de los cambios en una década, 2010 a 2020. Equilibrio Econ Nueva Época Rev Econ Política Soc 17:83–109
- Pérez Medina S (2011) Políticas públicas de combate a la pobreza en Yucatán, 1990–2006. Gest Política Pública 20:291–329
- Pielke RA, Rubiera J, Landsea C et al (2003) Hurricane vulnerability in latin America and the Caribbean: normalized damage and loss potentials. Nat Hazards Rev 4:101–114. [https://doi.org/10.1061/\(ASCE\)1527-6988\(2003\)4:3\(101\)](https://doi.org/10.1061/(ASCE)1527-6988(2003)4:3(101))

- Pita GL, Pinelli J-P, Gurley KR, Hamid S (2013) Hurricane vulnerability modeling: development and future trends. *J Wind Eng Ind Aerodyn* 114:96–105
- Ramírez-Carrillo LA (2020) The thin broken line. history, society, and the environment on the Yucatan Peninsula. In: Azcorra, H., Dickinson, F. (eds) *Culture, Environment and Health in the Yucatan Peninsula*. Springer, Cham, pp 9–36. https://doi.org/10.1007/978-3-030-27001-8_2
- Rivera-Monroy VH, Farfán LM, Brito-Castillo L et al (2020) Tropical cyclone landfall frequency and large-scale environmental impacts along Karstic Coastal Regions (Yucatan Peninsula, Mexico). *Appl Sci Switz* 10:5815. <https://doi.org/10.3390/app10175815>
- Romero D, Alfaro E, Orellana R, Hernandez Cerda M-E (2020) Standardized drought indices for pre-summer drought assessment in Tropical Areas. *Atmosphere* 11:1209. <https://doi.org/10.3390/atmos11111209>
- Ruiz-Salcines P, Salles P, Robles-Díaz L et al (2019) On the use of parametric wind models for wind wave modeling under Tropical cyclones. *Water* 11:2044. <https://doi.org/10.3390/w11102044>
- Sánchez Triana E, Ruitenbeek J, Enriquez S, et al (2016) Green and inclusive growth in the Yucatan Peninsula. *Int Bank Reconstr Dev World Bank Rep No AUS6091*
- Sánchez-Rivera G, Frausto-Martínez O, Gómez-Mendoza L et al (2021) Tropical cyclones in the North Atlantic Basin and Yucatan Peninsula, Mexico: identification of extreme events. *Int J Des Nat Ecodynamics* 16:145–160. <https://doi.org/10.18280/ijdne.160204>
- Sheng YP, Zou R (2017) Assessing the role of mangrove forest in reducing coastal inundation during major hurricanes. *Hydrobiologia* 803:87–103. <https://doi.org/10.1007/s10750-017-3201-8>
- Shi P, Ye T, Wang Y et al (2020) Disaster risk science: a geographical perspective and a research framework. *Int J Disaster Risk Sci* 11:426–440. <https://doi.org/10.1007/s13753-020-00296-5>
- Siagian TH, Purhadi P, Suhartono S, Ritonga H (2014) Social vulnerability to natural hazards in Indonesia: driving factors and policy implications. *Nat Hazards* 70:1603–1617
- Soares D, Millán G, Gutiérrez I (2014) Reflexiones y expresiones de la vulnerabilidad social en el sureste de México. *Instituto Mexicano de Tecnología del Agua*
- Tenzing JD (2020) Integrating social protection and climate change adaptation: a review. *Wiley Interdiscip Rev Clim Change* 11:e626
- Terray L (2012) Evidence for multiple drivers of North Atlantic multi-decadal climate variability. *Geophys Res Lett*. <https://doi.org/10.1029/2012GL053046>
- Touma D, Stevenson S, Camargo SJ et al (2019) Variations in the intensity and spatial extent of tropical cyclone precipitation. *Geophys Res Lett* 46:13992–14002. <https://doi.org/10.1029/2019GL083452>
- Xi D, Lin N, Smith J (2020) Evaluation of a physics-based tropical cyclone rainfall model for risk assessment. *J Hydrometeorol* 21:2197–2218. <https://doi.org/10.1175/JHM-D-20-0035.1>
- Zamudio-Sánchez FJ, Soriano-Montero M, Ibarra-Contreras P (2012) Análisis sobre la evolución del desarrollo humano en la península de Yucatán. *Econ Soc Territ* 12:543–596. <https://doi.org/10.22136/est00201262>
- Zhou Y, Li N, Wu W et al (2014) Local spatial and temporal factors influencing population and societal vulnerability to natural disasters: population and societal vulnerability to natural disasters. *Risk Anal* 34:614–639. <https://doi.org/10.1111/risa.12193>
- Zúñiga RAA, Villoria AMG (2018) Desastres en México de 1900 a 2016: patrones de ocurrencia, población afectada y daños económicos. *Rev Panam Salud Pública* 42:e55

Publisher's Note Springer Nature remains neutral with regard to jurisdictional claims in published maps and institutional affiliations.